OSBP-related protein 4L promotes phospholipase Cβ3 translocation from the nucleus to the plasma membrane in Jurkat T-cells

Received for publication, August 21, 2018, and in revised form, September 6, 2018 Published, Papers in Press, September 20, 2018, DOI 10.1074/jbc.RA118.005437

Guoping Pan[‡1], Xiuye Cao[‡1], Bo Liu[‡], Chaowen Li[‡], Dan Li[‡], Jie Zheng[‡], Chaofeng Lai[‡], Vesa M. Olkkonen[§], Wenbin Zhong[‡2], and Daoguang Yan[‡3]

From the [‡]Department of Biology, Jinan University, Guangzhou 510632, China and [§]Minerva Foundation Institute for Medical Research, Biomedicum 2U, FI-00290 Helsinki, Finland

Edited by George M. Carman

Phosphoinositide phospholipases C (PLCs) are a family of eukaryotic intracellular enzymes with important roles in signal transduction. In addition to their location at the plasma membrane, PLCs also exist within the cell nucleus where they are stored. We previously demonstrated that OSBP-related protein 4L (ORP4L) anchors cluster of differentiation 3ε (CD3ε) to the heterotrimeric G protein subunit ($G\alpha_{q/11}$) to control PLCβ3 relocation and activation. However, the underlying mechanism by which ORP4L facilitates PLCβ3 translocation remains unknown. Here, using confocal immunofluorescence microscopy and coimmunoprecipitation assays, we report that ORP4L stimulates PLCβ3 translocation from the nucleus to the plasma membrane in Jurkat T-cells in two steps. First, we found that ORP4L is required for the activation of Ras-related nuclear protein (RAN), a GTP-binding nuclear protein that binds to exportin 1 and eventually promotes the nuclear export of PLCβ3. Second, we also observed that ORP4L interacts with vesicle-associated membrane protein–associated protein A (VAPA) through its two phenylalanines in an acidic tract (FFAT) motif. This complex enabled PLCβ3 movement to the plasma membrane, indicating that PLCβ3 translocation occurs in a VAPA-dependent manner. This study reveals detailed mechanistic insight into the role of ORP4L in PLCβ3 redistribution from storage within the nucleus to the plasma membrane via RAN activation and interaction with VAPA in Jurkat T-cells.

Phosphoinositide phospholipases C (PLCs)[4] are a family of eukaryotic intracellular enzymes that play important roles in signal transduction processes (1). PLCs cleave their substrate phosphatidylinositol 4,5-bisphosphate (PIP_2) present in the inner leaflet of the plasma membrane to generate the second messengers inositol 1,4,5-trisphosphate (IP_3) and diacylglycerol, which go on to alter cell responses such as proliferation, differentiation, apoptosis, cytoskeleton remodeling, vesicular trafficking, ion channel conductance, endocrine function, and neurotransmission (2, 3). It is important to note that, except the plasma membrane, PLCs also exist within other subcellular regions such as the cytoplasm and nucleus of the cell (4–6).

Oxysterol-binding protein (OSBP) is a cytoplasmic protein with a high affinity for oxysterols (7). In humans, 12 genes encode a family of proteins characterized by a C-terminal OSBP-related ligand-binding domain (ORD) (8) that binds oxysterols or cholesterol (9, 10). Recent work shows that certain ORPs also have the capacity to bind and transport glycerophospholipids including phosphoinositides, which might be a key feature of their function (11–13). In addition to a ligand-binding domain, a majority of the ORPs carry a pleckstrin homology (PH) domain that targets organelle membranes via phosphoinositides and a motif designated two phenylalanines in an acidic tract (FFAT) motif (14–16), targeting the endoplasmic reticulum (ER) via VAMP-associated proteins (VAPs). VAPs are type II integral membrane proteins of the ER that function as regulators of membrane trafficking, lipid metabolism and transport, microtubule organization, and the unfolded protein response (17–19).

ORP4 (also known as OSBP2) is present as two major variants designated as ORP4L and ORP4S (20). ORP4L was reported in early studies to be detected in peripheral blood leukocytes from patients with chronic myeloid leukemia but not healthy donors (21, 22) and is implicated as a potential marker for solid tumor dissemination and poor prognosis (21). Furthermore, ORP4L was found to be involved in tumor cell proliferation (23). Our recent work showed that ORP4L interacts directly with CD3ε, $G\alpha_{q/11}$, and PLCβ3; scaffolds the translo-

This work was supported by grants from the Basic Research Program of Guangdong province, China (Grant 2017A030308002 to D. Y.) and National Natural Science Foundation of China (NSFC) (Grants 81770438, 91439122, and 30971104 to D. Y.); Academy of Finland Grant 285223 (to V. M. O.); and the Sigrid Juselius Foundation, the Magnus Ehrnrooth Foundation, and the Finnish Foundation for Cardiovascular Research (to V. M. O.). The authors declare that they have no conflicts of interest with the contents of this article.

This article contains Figs. S1 and S2.

[1] Both authors contributed equally to this work.

[2] To whom correspondence may be addressed. Tel.: 86-20-85222993; E-mail: twbzhong@jnu.edu.cn.

[3] To whom correspondence may be addressed. Tel.: 86-20-85222993; Fax: 86-20-85220219; E-mail: tydg@jnu.edu.cn.

[4] The abbreviations used are: PLC, phosphoinositide phospholipase C; ORP4L, OSBP-related protein 4L; PIP_2, phosphatidylinositol 4,5-bisphosphate; IP_3, inositol 1,4,5-trisphosphate; OSBP, oxysterol-binding protein; ORD, OSBP-related ligand-binding domain; VAP, VAMP-associated protein; T-ALL, acute T-lymphoblastic leukemia; NLS, nuclear localization signal; NES, nuclear export signal; GST, glutathione *S*-transferase; VAMP, vesicle-associated membrane protein; LMB, leptomycin B; CD3, cluster of differentiation 3; RAN, Ras-related nuclear protein; FFAT, two phenylalanines in an acidic tract; ER, endoplasmic reticulum; p-PLCβ3, phosphorylated PLCβ3; PM, plasma membrane; H+L, heavy + light chains; FBS, fetal bovine serum; HRP, horseradish peroxidase.

cation of PLCβ3 from the nucleus to the plasma membrane; and regulates its activation to promote IP_3 production. In this manner, ORP4L serves to regulate IP_3-induced Ca^{2+} signaling, mitochondrial respiration, and ATP generation and thereby maintains the survival of acute T-lymphoblastic leukemia (T-ALL) cells (24). However, the detailed pathway through which ORP4L mediates the translocation of intranuclear PLCβ3 remains to be identified.

Ras-related nuclear protein (RAN), also known as the GTP-binding nuclear protein RAN, is involved in the transport of proteins across the nuclear envelope by interacting with karyopherins and changing their ability to bind or release cargos. Cargo proteins containing a nuclear localization signal (NLS) are transported into the nucleus by binding importins. Inside the nucleus, RAN-GTP binds to importin and releases the import cargo. Cargo that needs to shift from the nucleus into the cytoplasm binds to exportin in a ternary complex with RAN-GTP. Upon hydrolysis of RAN-GTP to RAN-GDP outside the nucleus, the complex dissociates, and the export cargo is released (25, 26). In this study, we reveal mechanistic insight into the role of ORP4L in PLCβ3 redistribution via RAN activation and VAPA involvement and offer a model for the shift of PLCβ3 from storage within the nucleus to its functional site.

Results

PLCβ3 exists in the nucleus of unstimulated cells

The localization of PLCβ3 in Jurkat T-cells was investigated by confocal immunofluorescence microscopy. In unstimulated Jurkat T-cells, PLCβ3 exhibited an intranuclear localization (Fig. 1*A*). The fractionation of Jurkat T-cells analyzed by Western blotting further confirmed that a majority of PLCβ3 protein localized in the nucleus (Fig. 1*B*). Consistent with the observations in Jurkat T-cells, a similar intranuclear localization of PLCβ3 was apparent in K562, HeLa, and HepG2 cells (Fig. 1*C*). The Human Protein Atlas website (available from: https://www.proteinatlas.org/ENSG00000149782-PLCB3/cell#human)[5] also provided the PLCβ3 intranuclear localization images in MCF-7, A-431, and U-2 OS cells (Fig. S1). Conversely, our recent study suggested that PLCβ3 catalyzes IP_3 production in T-ALL cells as opposed to PLCγ1 in normal T-cells cells (24). When we compared the PLCβ3 protein level, we found significantly up-regulated expression of this protein in primary T-ALL cells and Jurkat T-cells as compared with normal T-cells (Fig. 1*D*). In contrast to intranuclear localization in T-ALL cells, confocal immunofluorescence showed that PLCβ3 is distributed at the peripheral plasma membrane in normal T-cells (Fig. 1*E*). These results indicated a pathway of T-ALL cells regulating PLCβ3 localization, which was different from normal T-cells.

It has been reported that the interaction between cargo molecules and the transport receptors is frequently mediated by short linear motifs on the cargo called NLSs or nuclear export signals (NESs) (27, 28). Therefore, we dissected the sequence of PLCβ3 with two online platforms, NLStradamus (http://www.moseslab.csb.utoronto.ca/NLStradamus/)[5] and NetNES (http://www.cbs.dtu.dk/services/NetNES/),[5] to discover its NLS and NES. By sequence analysis with NLStradamus (29), we found that PLCβ3 contains two potential NLS sequences within amino acids 466–485 and 967–984 (Fig. 1*F*). Furthermore, the NetNES 1.1 Server (30) predicts that amino acids 310–315 within PLCβ3 constitute a leucine-rich nuclear export signal (Fig. 1*G*). These data indicated that the intranuclear localization of PLCβ3 in unstimulated cells is under the control of nuclear import/export machineries, which finally determine its subcellular distribution.

ORP4L facilities PLCβ3 translocation and activation by binding PLCβ3

We previously identified that ORP4L in fact interacts physically with PLCβ3 (24). These previous results suggested that PLCβ3 may be sequestered in the nucleus under unstimulated conditions and upon anti-CD3 stimulation is translocated to the plasma membrane in the presence of ORP4L, thereby gaining access to its substrate, PIP_2 (Fig. S2, *A* and *B*).

A coimmunoprecipitation assay showed that ORP4L interacts specifically with PLCβ3 but not with other isotypes of PLCβs in Jurkat T-cells (Fig. S2*C*). PLCβ3 knockdown (Fig. 2*A*) significantly reduced IP_3 production and Ca^{2+} release from the ER upon anti-CD3 stimulation (Fig. 2*B*), indicating its dominant role in Jurkat T-cells. ORP4L overexpression promoted IP_3 production and Ca^{2+} release, effects reduced in PLCβ3 knockdown cells (Fig. 2, *C* and *D*). ORP4L binds PLCβ3 via its amino acid region 445–513 (31). To investigate the role of this physical interaction, we generated a truncated ORP4L protein lacking the PLCβ3-binding region (ORP4L Δ445–513). ORP4L overexpression enabled PLCβ3 translocation from the nucleus to the plasma membrane, but ORP4L Δ445–513 failed to do this (Fig. 2*E*). Phosphorylation at Ser^{537} contributes to the basal activity of PLCβ3 (32). Consequently, ORP4L but not ORP4L Δ445–513 increased PLCβ3 activity (Fig. 2, *E* and *F*; phosphorylation of PLCβ3), IP_3 production, and Ca^{2+} release (Fig. 2*G*). Confocal imaging showed that p-PLCβ3 was present only at the plasma membrane, and not in the nucleus, when cells were stimulated with anti-CD3 (Fig. 2*E*), indicating a sequestering of PLCβ3 in the nucleus in its inactive state. These results suggested that PLCβ3 translocation and activation are dependent on its direct interaction with ORP4L.

ORP4L activates RAN in Jurkat T-cells for PLCβ3 exportation from the nucleus

The small GTPase RAN plays a central role in the coordination and trafficking of nuclear proteins (33, 34). To investigate mechanisms of PLCβ3 export, we performed RAN activity assays. As expected, anti-CD3 stimulation increased the active form of RAN (RAN-GTP) in a time-dependent manner (Fig. 3*A*), whereas RAN activity declined in ORP4L knockdown cells (Fig. 3*B*), indicating that ORP4L is required for RAN activation in Jurkat T-cells upon anti-CD3 stimulation. Anti-CD3 stimulation led to phosphorylation of PLCβ3 in a time-dependent manner (Fig. 3*C*). Leptomycin B (LMB), a specific inhibitor of exportin 1 (34, 35), was added simultaneously with anti-CD3 and blocked the nuclear export of PLCβ3 (Fig. 3*E*) as well as the phosphorylation of PLCβ3 at the plasma membrane (Fig. 3, *D*

[5] Please note that the JBC is not responsible for the long-term archiving and maintenance of this site or any other third party-hosted site.

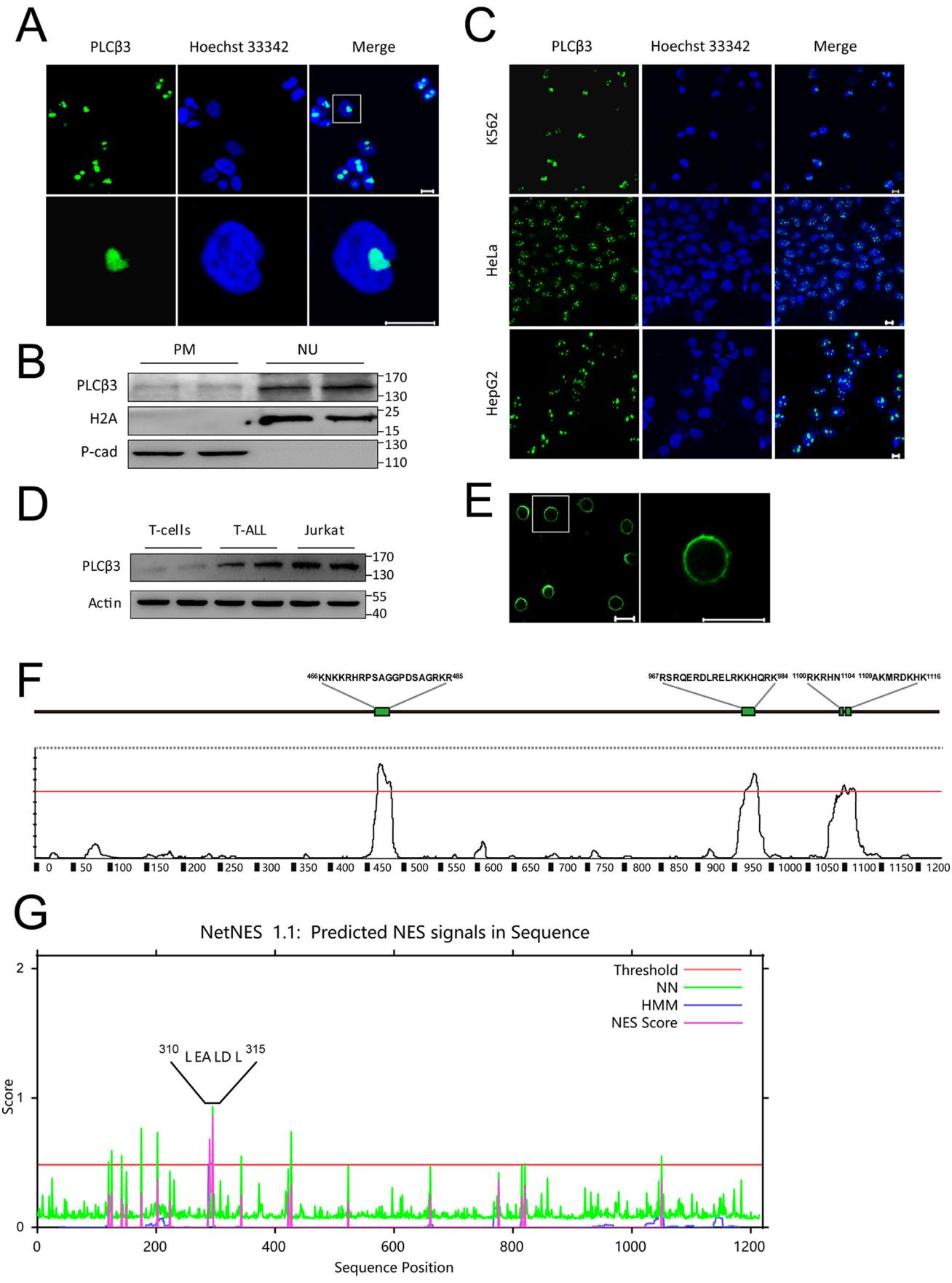
A
PLCβ3
Hoechst 33342
Merge
B
PM
NU
PLCβ3
H2A
P-cad
170
130
25
15
130
110
C
PLCβ3
Hoechst 33342
Merge
K562
HeLa
HepG2
D
T-cells
T-ALL
Jurkat
PLCβ3
Actin
170
130
55
40
E
F
466KNKKRHRPSAGGPDSAGRKR485
967RSRQERDLRELRKKHQRK984 1100RKRHN1104 1109AKMRDKHK1116
0 50 100 150 200 250 300 350 400 450 500 550 600 650 700 750 800 850 900 950 1000 1050 1100 1150 1200
G
NetNES 1.1: Predicted NES signals in Sequence
Threshold
NN
HMM
NES Score
310 LEALDL 315
Score
Sequence Position
0 200 400 600 800 1000 1200
0 1 2

and *E*). Furthermore, LMB treatment abolished PLCβ3 activation (Fig. 4, *A* and *B*), IP_3 production, and Ca^{2+} release (Fig. 4*C*) upon ORP4L overexpression. These results suggest that ORP4L enables transduction of CD3 signaling to RAN and PLCβ3 activation in Jurkat T-cells dependent on exportin 1.

ORP4L interacts with VAPA and functions in PLCβ3 transport

The next question is how PLCβ3 is transported to the cell periphery. Because yeast ORPs (Osh proteins) and VAPs assemble at ER–plasma membrane contact sites to control the metabolism of plasma membrane phosphoinositides (36) and VAPs interact with microtubules, which play crucial roles in the maintenance and organization of cellular organelles as well as in membrane trafficking (19), we hypothesized that the VAPA may be involved in the translocation of PLCβ3.

ORP4L, via bimolecular fluorescence complementation, was shown to form a complex with its ER receptor, VAPA, in mammalian cells (14), but there is no direct evidence for the endogenous ORP4L and VAPA interaction. We next sought to investigate whether endogenous ORP4L interacts with VAPA in Jurkat T-cells. Collectively, the confocal immunofluorescence revealed colocalization between endogenous ORP4L and VAPA (Fig. 5*A*); moreover, the coimmunoprecipitation experiments showed that ORP4L interacted with the integral membrane protein VAPA (Fig. 5*B*). The GST pulldown experiments further confirmed that WT ORP4L directly interacts with VAPA, whereas the ORP4L lacking the FFAT motif did not (Fig. 5*C*). These data suggest that ORP4L directly interacts with VAPA via its FFAT motif.

To further dissect the functional role of ORP4L in PLCβ3 translocation and activation, we transfected Jurkat T-cells with full-length ORP4L or truncated ORP4L lacking the FFAT motif (ORP4L ΔFFAT). Confocal immunofluorescence microscopy images showed that p-PLCβ3 clearly occurred in the cell periphery in ORP4L-overexpressing cells, but this could not be observed in cells overexpressing ORP4L devoid of the FFAT motif (Fig. 5*D*). Accordingly, the results of Western blot analysis confirmed the enhanced PLCβ3 phosphorylation in cells overexpressing WT ORP4L but not in cells expressing ORP4L that lacks the FFAT motif (Fig. 5, *E* and *F*).

Next, we measured the IP_3 production and Ca^{2+} release from ER upon anti-CD3 stimulation in Jurkat T-cells. The results showed that ORP4L overexpression promotes IP_3 production and Ca^{2+} release (Fig. 5, *G* and *H*). To our surprise, in contrast to its effect on PLCβ3 activation, the ORP4L ΔFFAT construct was able to increase the IP_3 and Ca^{2+} response (Fig. 5, *G* and *H*), although to a lower extent compared with full-length ORP4L. PIP_2 located in the plasma membrane acts as substrate for PLC catalysis (38). Recently, an important role of the ORD of ORPs as a transporter for PIP_2 has been explored (39). We hypothesized that the PLCβ3 reaction may require the ORD of ORP4L to transport the substrate PIP_2. Although ORP4L ΔFFAT fails to facilitate PLCβ3 translocation, the ORD remaining enhances the PIP_2 transport for plasma membrane (PM) PLCβ3 catalysis. To this end, we constructed truncated ORP4L lacking FFAT and ORD (ORP4L ΔFFAT&ORD). Compared with full-length ORP4L, ORP4L ΔFFAT&ORD could not increase PLCβ3 activation or evoke the IP_3 and Ca^{2+} response (Fig. 5, *G* and *H*), indicating the requirement of the ORD for PLCβ3 catalysis.

To further investigate the potential dependence of PLCβ3 translocation on VAPA, RNAi was used to inhibit VAPA expression. The translocation of PLCβ3 to a peripheral location upon anti-CD3 treatment was prevented by knockdown of VAPA (Fig. 6*A*), indicating a role of the ORP4L–VAPA complex in controlling PLCβ3 localization and activity. Moreover, PLCβ3 could not be shifted to its phosphorylated form in VAPA knockdown Jurkat T-cells, even when ORP4L was overexpressed (Fig. 6, *B* and *C*). These results suggested that the nuclear pool of PLCβ3 in unstimulated Jurkat T-cells is mobilized to the plasma membrane in a manner dependent on the ORP4L–VAPA complex.

Discussion

We recently reported that ORP4L organizes a signaling complex involving the translocation and activation of nuclear, ER, mitochondrial, and plasma membrane molecular components (24). However, the detailed role of ORP4L in the shift of PLCβ3 from the nucleus to plasma membrane remained unclear. The present study offers evidence that the underlying mechanism of PLCβ3 translocation promoted by ORP4L is related to RAN activation and assistance by the ER receptor for ORP4L, VAPA (Fig. 6*D*).

PLCs perform a catalytic function at the plasma membrane where their substrate, PIP_2, is localized. However, PLCs also exist at other subcellular locations such as the cytoplasm and the nucleus (40–43). This separation of an enzyme from its substrates provides a regulatory mechanism, but understanding how the key molecules and translocation events control the function of PLCs requires new insights. In this study, we found that under unstimulated conditions PLCβ3 mainly exists within the Jurkat T-cell nucleus but translocates to the plasma membrane upon anti-CD3 stimulation. Colocalization of ORP4L and PLCβ3 was observed in Jurkat T-cells stimulated with anti-CD3, and the two proteins were found to interact physically, which prompted us to consider a role for ORP4L in the PLCβ3 plasma membrane translocation. Indeed, depletion of ORP4L significantly inhibited the shift of PLCβ3 to the plasma membrane, consistent with an important role of ORP4L in controlling the distribution and activity of PLCβ3 in T-ALL cells.

Figure 1. Localization of PLCβ3 in unstimulated cells. *A*, immunofluorescence staining with anti-PLCβ3 showing nuclear localization of the protein in Jurkat T-cells. *Scale bars*, 10 μm. *B*, Western blot analysis of PLCβ3 in PM and nuclear (*NU*) fractions of Jurkat T-cells. P-cadherin (*P-cad*) and histone H2A were used as loading controls for the plasma membrane and nuclear fractions, respectively. *C*, immunofluorescence staining with anti-PLCβ3 showing nuclear localization of the protein in K562, HeLa, and HepG2 cells. *Scale bars*, 10 μm. *D*, Western blot showing PLCβ3 expression in normal T-cells, primary T-ALL cells, and Jurkat T-cells. *E*, immunofluorescence staining with anti-PLCβ3 showing plasma membrane localization of PLCβ3 in normal T-cells. *Scale bars*, 10 μm. *F*, prediction of NLS sequences in PLCβ3 with NLStradamus (http://www.moseslab.csb.utoronto.ca/NLStradamus/). *G*, prediction of a NES sequence in PLCβ3 with NetNES 1.1 Server (http://www.cbs.dtu.dk/services/NetNES/). *HMM*, hidden Markov model; NN, *NetNES 1.1*. (Please note that the JBC is not responsible for the long-term archiving and maintenance of this site or any other third party-hosted site.)

We have previously provided evidence that ORP4L can specifically interact with CD3ϵ, $G\alpha_{q/11}$, and PLCβ3, and these interactions were modestly enhanced upon anti-CD3 stimulation, suggesting a dynamic nature of the complex formation that is under the control of CD3 signaling (24). Therefore, we hypothesize that formation of the CD3ϵ–$G\alpha_{q/11}$ complex scaf-

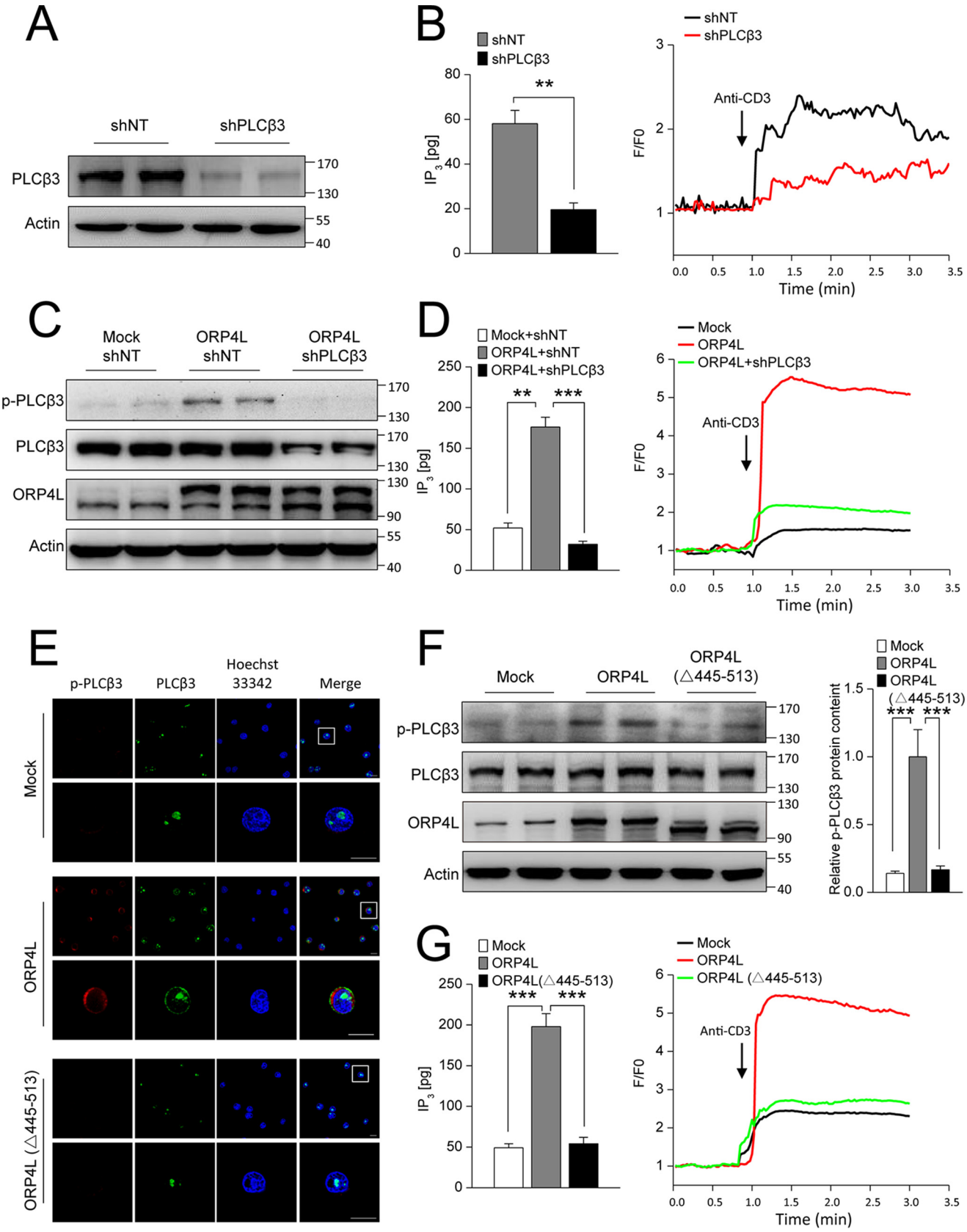

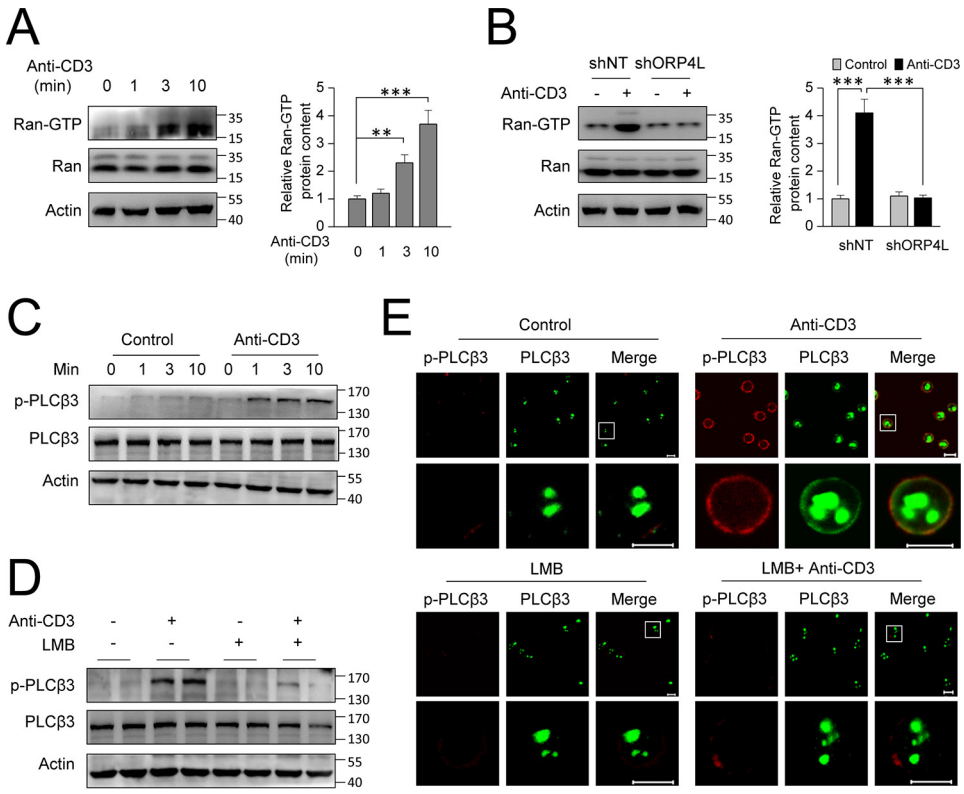

Figure 3. Anti-CD3 stimulation activates RAN for PLCβ3 exportation from the nucleus in Jurkat T-cells. *A*, the active form of RAN (RAN-GTP) in Jurkat T-cells upon anti-CD3 stimulation. Cells were stimulated for the indicated times with 10 μg ml^{-1} anti-CD3. *B*, the active form of RAN (RAN-GTP) in Jurkat T-cells with ORP4L knockdown upon anti-CD3 stimulation. Cells were stimulated for 3 min with 10 μg ml^{-1} anti-CD3 for 3 min. The relative GTP-RAN protein content was quantified from Western blots and normalized with the β-actin signal. *C* and *D*, Jurkat T-cells were stimulated for the indicated times with 10 μg ml^{-1} anti-CD3 (*C*) or preincubated for 2 h with 50 ng ml^{-1} LMB (*D*) followed by 5-min stimulation with 10 μg ml^{-1} anti-CD3, and PLCβ3 phosphorylation at Ser^{537} was analyzed by Western blotting. *E*, confocal microscopy analysis of PLCβ3 and p-PLCβ3 in Jurkat T-cells after 5-min anti-CD3 stimulation (10 μg ml^{-1}) in the presence or absence of LMB. *Scale bars*, 10 μm. The data represent mean ± S.D. from an experiment performed in triplicate. **, $p < 0.01$; ***, $p < 0.001$, Student's *t* test. All *error bars* represent S.D. *NT*, nontargeting.

folded by ORP4L enhances $G\alpha_{q/11}$ activity for activating RAN and PLCβ3 upon anti-CD3 stimulation. The increase in active RAN (RAN-GTP) upon anti-CD3 stimulation and the reduction of the shift of PLCβ3 by leptomycin B, an inhibitor of exportin 1, suggest that PLCβ3 trafficking from the nucleus is mediated by the exportin system.

ORP4L plays an important role in controlling the distribution and activity of PLCβ3 in Jurkat T-cells and primary T-ALL cells (24). The specific nature of this inhibition was further corroborated by data showing that depletion of VAPA, the ER membrane receptor of ORP4L, had a similar effect as depletion of ORP4L. We envision that the deletion of VAPA results in the dysfunction of ORP4L in regulation of PLCβ3 translocation in Jurkat T-cells.

Moreover, our recent findings showing that ORP4L binds PIP_2 are consistent with a model in which an ORP4L–VAPA complex may target PLCβ3 to distinct PIP_2-containing microdomains at the plasma membrane (44, 45). The observed affinity of ORP4L for PIP_2, the major plasma membrane phosphoinositide (46), together with an interaction with PLCβ3 suggests an association of ORP4L with components of the plasma membrane. In contrast, interaction with VAPA, an integral membrane protein mainly found in the ER (19), targets ORP4L to ER membranes. This duality in membrane targeting may indicate that ORP4L has the capacity to simultaneously associate with the ER and the plasma membrane. In fact, ORP4L was found to colocalize with PLCβ3 at punctate peripheral sites, which could represent ER–plasma membrane contacts (47). Such regions are commonly referred to as "puncta" (48), and it is within the puncta that key signaling occurs during T-cell activation (49). Such contact sites are also known to play crucial roles in Ca^{2+} regulation during store-operated Ca^{2+} entry and muscle excitation-contraction coupling (37). Our findings thus raise the possibility that ORP4L may operate to coordinate the activity of PLCβ3 at ER–plasma membrane contacts.

Figure 2. ORP4L binding is required for PLCβ3 translocation and activation in Jurkat T-cells. *A*, Western blot showing PLCβ3 knockdown in Jurkat T-cells. *B*, IP_3 production and Ca^{2+} release upon anti-CD3 stimulation (10 μg ml^{-1}) in Jurkat T-cells with PLCβ3 knockdown. *C*, Western blot showing PLCβ3 knockdown and ORP4L overexpression in Jurkat T-cells. *D*, IP_3 production and Ca^{2+} release upon anti-CD3 stimulation (10 μg ml^{-1}) in Jurkat T-cells upon the indicated genetic manipulations. *E*, confocal microscopy analysis of the location of p-PLCβ3 phosphorylated at Ser^{537} in control, ORP4L-, or ORP4L Δ445–513-overexpressing cells. *Scale bars*, 10 μm. *F*, Western blot analysis of PLCβ3 phosphorylation at Ser^{537} in control, ORP4L-, or ORP4L Δ445–513-overexpressing cells. The relative p-PLCβ3 protein content was quantified from Western blots and normalized with the β-actin signal. *G*, IP_3 production and Ca^{2+} response upon anti-CD3 stimulation (10 μg ml^{-1}) in Jurkat T-cells overexpressing the indicated constructs. The data represent mean ± S.D. from an experiment performed in triplicate. **, $p < 0.01$; ***, $p < 0.001$, Student's *t* test. All *error bars* represent S.D. *NT*, nontargeting.

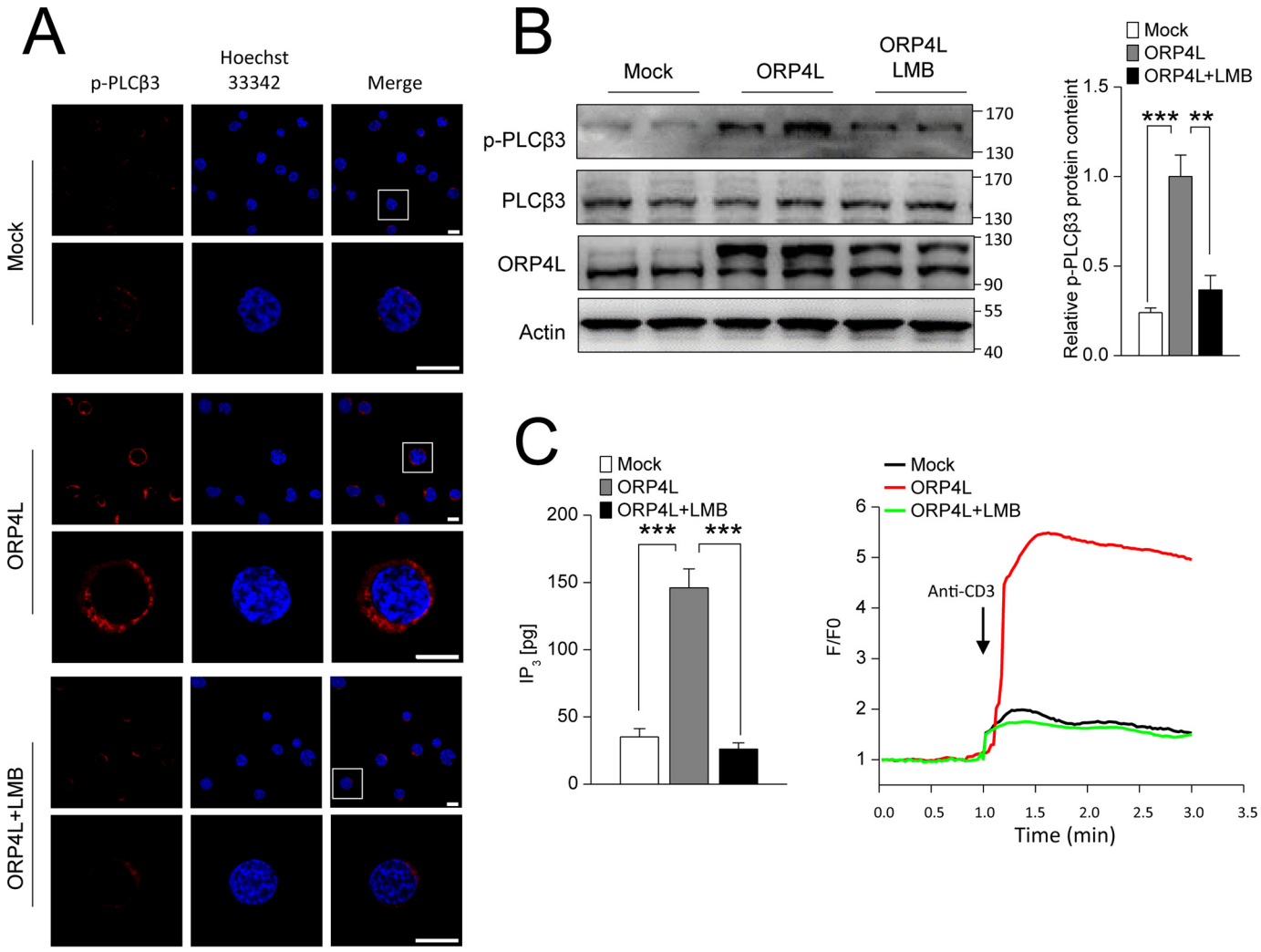

Figure 4. LMB inhibits the function of ORP4L in PLCβ3 activation. *A*, confocal microscopy analysis of PLCβ3 phosphorylated at Ser^{537} in control and ORP4L-overexpressing cells in the presence or absence of 50 ng ml^{-1} LMB. *Scale bars*, 10 μm. *B*, Western blot analysis of PLCβ3 phosphorylation in control and ORP4L-overexpressing cells in the presence or absence of 50 ng ml^{-1} LMB. The relative p-PLCβ3 protein content was quantified from Western blots and normalized with the β-actin signal. *C*, IP_3 production and Ca^{2+} response upon anti-CD3 stimulation (10 μg ml^{-1}) in control and ORP4L overexpressing cells in the presence or absence of 50 ng ml^{-1} LMB. The data represent mean ± S.D. from an experiment performed in triplicate. **, $p < 0.01$; ***, $p < 0.001$, Student's *t* test. All *error bars* represent S.D.

In conclusion, our results suggest that ORP4L facilitates PLCβ3 translocation in T-ALL cells. RAN activation under control of ORP4L regulates the export of inactive PLCβ3 from the nucleus, and interaction of VAPA with ORP4L mediates PLCβ3 transport to the cell periphery. Our study offers novel mechanistic insight into ORP4L functions in T-ALL cells. It also provides a model for a shift of PLCβ from subcellular storage to its functional site via RAN activation and VAPA function.

Experimental procedures

Reagents and antibodies

Alexa Fluor 488 goat anti-mouse IgG (catalogue number A-11001), Alexa Fluor 546 goat anti-rabbit IgG (catalogue number A-11035), and Alexa Fluor 647 donkey anti-goat IgG (catalogue number A-21447) were purchased from Invitrogen. LEAF purified human anti-CD3 (clone HIT3a, catalogue number 300314) and anti-H2A (catalogue number 613301) were purchased from BioLegend (San Diego, CA). Hoechst 33342 and anti-ORP4L (catalogue number HAP021514) were purchased from Sigma-Aldrich. Anti-PLCβ3 (catalogue number Nosc-133231), anti-pan-cadherin (catalogue number sc-1499), and anti-VAPA (catalogue number sc-48698) were from Santa Cruz Biotechnology (Santa Cruz, CA). Anti-p-PLCβ3 (catalogue number 2481) was purchased from Cell Signaling Technology (Beverly, MA). Anti-actin (catalogue number 60008-1), HRP-conjugated AffiniPure goat anti-mouse IgG (H+L) (catalogue number SA00001-1), HRP-conjugated AffiniPure goat anti-rabbit IgG (H+L) (catalogue number SA00001-2), and HRP-conjugated AffiniPure donkey anti-foat IgG (H+L) (catalogue number SA00001-3) were purchased from Proteintech Group (Chicago, IL).

Human leukocyte specimens and cell lines

Fresh leukocytes were isolated from peripheral blood of healthy human donors and T-ALL patients after obtaining written informed consent. Naive CD3$^+$ T-cells were isolated using an Enhanced Human T Cell Recovery Column kit (Cedarlane, Burlington, Ontario, Canada) according to the manu-

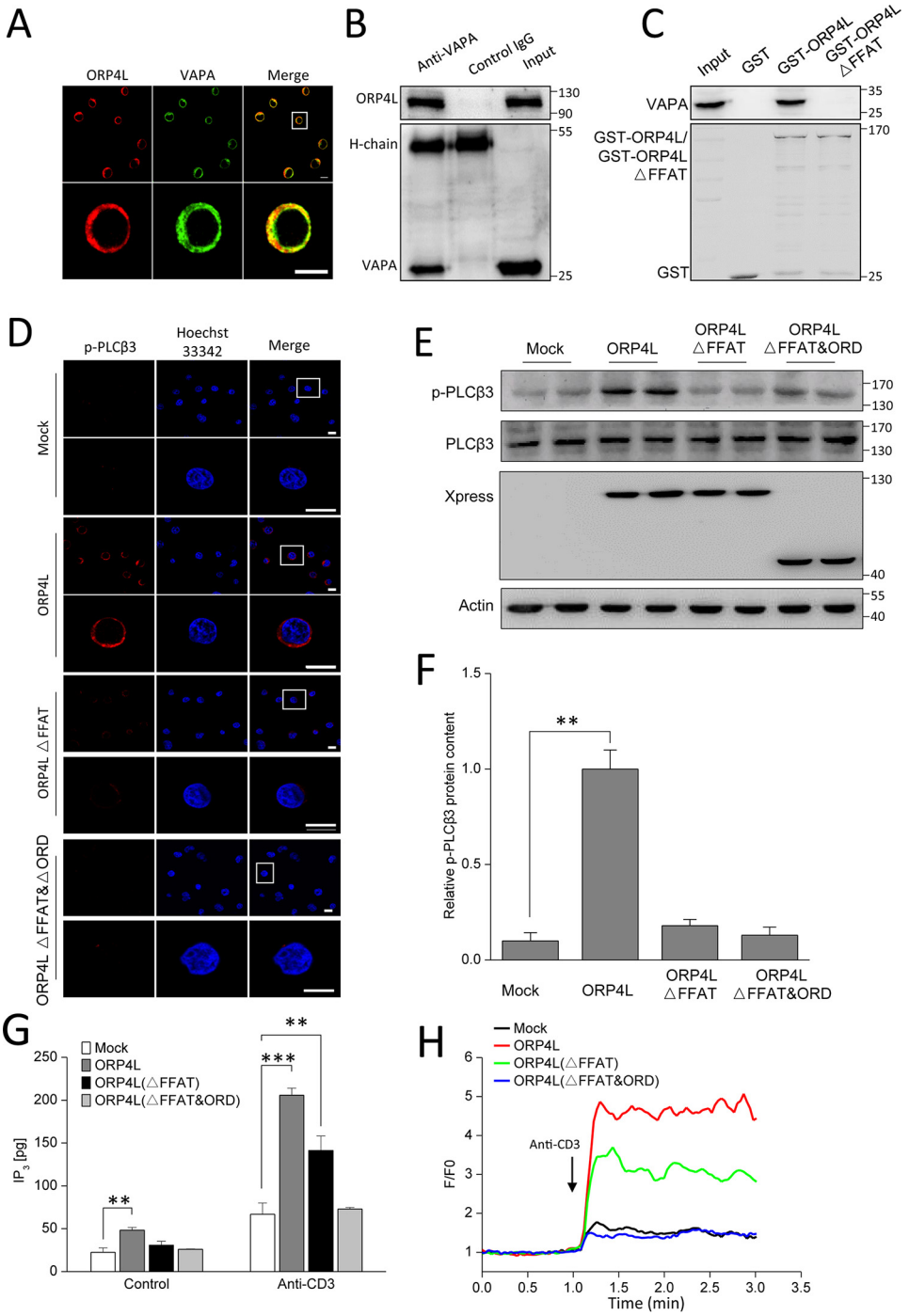

Figure 5. ORP4L interacts with VAPA to promote the transport of PLCβ3. *A*, confocal microscopy analysis of the colocalization between endogenous ORP4L (*red*) and VAPA (*green*) in Jurkat T-cells. *Scale bars*, 10 μm. *B*, Western blots showing coimmunoprecipitation of endogenous ORP4L and VAPA from Jurkat T-cells. *C*, GST pulldown experiments with bacterially expressed GST-ORP4L, GST-ORP4L ΔFFAT, and endogenous VAPA from Jurkat T-cells. *D*, confocal microscopy analysis of the location of p-PLCβ3 phosphorylated at Ser^{537} in control, ORP4L-, ORP4L ΔFFAT-, or ORP4L ΔFFAT&ORD-overexpressing cells. *Scale bars*, 10 μm. *E*, Western blot analysis of PLCβ3 phosphorylation at Ser^{537} in control, ORP4L-, ORP4L ΔFFAT-, or ORP4L ΔFFAT&ORD-overexpressing cells. *F*, the relative p-PLCβ3 protein content was quantified from Western blots (*B*) and normalized with the β-actin signal. *G* and *H*, IP_3 production (*G*) and Ca^{2+} response (*H*) upon anti-CD3 stimulation (10 μg ml^{-1}) in Jurkat T-cells overexpressing the indicated constructs. The data represent mean ± S.D. from an experiment performed in triplicate. **, $p < 0.01$; ***, $p < 0.001$, Student's *t* test. All *error bars* represent S.D. *H-chain*, heavy chain.

facturer's instruction. Jurkat T-cells, K562, HeLa, and HepG2 cells were purchased from American Type Culture Collection. Jurkat T-cells and K562 cells were maintained in RPMI 1640 medium containing 10% FBS, 100 units ml^{-1} penicillin, and 100 μg ml^{-1} streptomycin. HeLa and HepG2 cells were maintained in Dulbecco's modified Eagle's medium containing 10% FBS, 100 units ml^{-1} penicillin, and 100 μg ml^{-1} streptomycin. All cells were cultured at 37 °C in a humidified incubator with 5% CO_2.

Plasmid constructs

Human full-length ORP4L cDNAs were amplified by PCR amplification (5′-ATTTCTAGAATGGGGAAAGCGG-

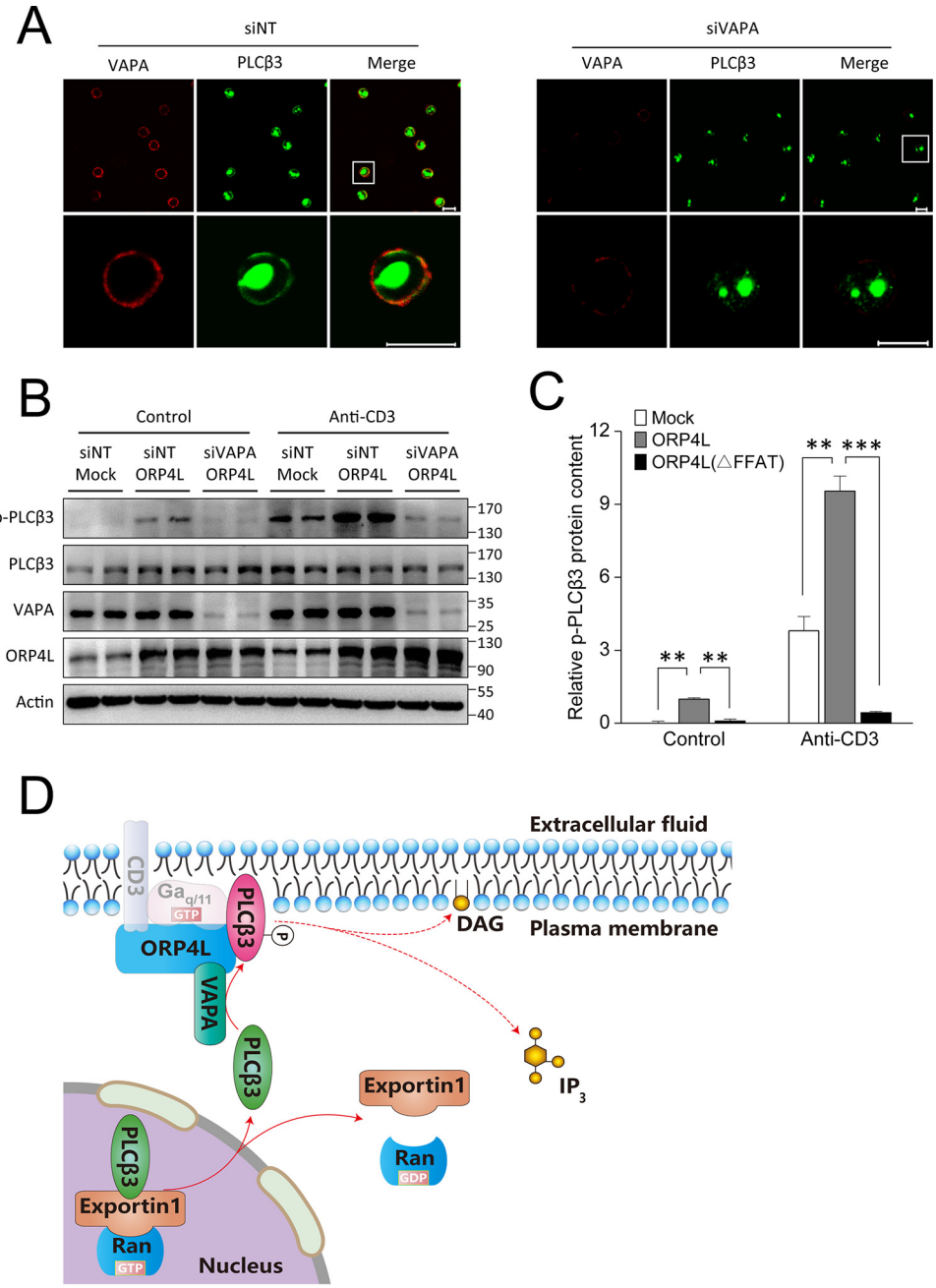

Figure 6. ORP4L loses the ability to enhance PLCβ3 transport in VAPA knockdown cells. *A*, PLCβ3 translocation to the PM in Jurkat T-cells transfected with nontargeting (*siNT*) or VAPA-specific (*siVAPA*) siRNA upon 5-min stimulation with 10 μg ml^{-1} anti-CD3 at 37 °C. Distribution of VAPA is displayed in *red*. *Scale bars*, 10 μm. *B*, PLCβ3 phosphorylation at Ser^{537} was analyzed by Western blotting in control and ORP4L-overexpressing cells in the presence or absence of VAPA knockdown. For anti-CD3 treatment, cells were stimulated for 5 min with 10 μg ml^{-1} anti-CD3 at 37 °C. *C*, the relative p-PLCβ3 protein content was quantified from Western blots (*B*) and normalized with the β-actin signal. The data represent mean ± S.D. from an experiment performed in triplicate. **, $p < 0.01$; ***, $p < 0.001$, Student's *t* test. All *error bars* represent S.D. *D*, a schematic model for the PLCβ3 shift from the nucleus to the plasma membrane. *DAG*, diacylglycerol.

CGGT-3′; 5′-ATTTCTAGAGTGGCGCTCAGAAGATGTT-GGGGCACATATGCCA-3′) from HeLa cell cDNA and subcloned into the pcDNA4HisMaxC (Invitrogen) vector. The FFAT motif deletion was generated by PCR from ORP4L cDNA with primers (Forward 1, 5′-ATTAGATCTATGGGGAAAG-CGGCGGCT-3′; Forward 450, 5′-TGATGAAGGATGTGG-AGTCTTCCATGGTATCTTCATCTTCCTCACTGTCC-3′; Reverse 916, 5′-ATTGTCGACGAAGATGTTGGGGCACA-TATGCCA-3′; Reverse 465, 5′-GGACAGTGAGGAAGATG-AAGATACATGGAAGACTCCACATCCTTCATCA-3′). All constructs were verified by sequencing.

Isolation of nuclear and plasma membrane fractions

Nuclear fractions were isolated using a nuclear/cytosol fractionation kit (Biovision) according to the manufacturer's instructions. Briefly, aliquots of 2 × 10^6 cells were collected by centrifugation followed by adding cytosol extraction buffer-A and homogenization. After cytosol extraction buffer-B was

added, the sample was centrifuged, and the supernatant fraction was obtained. The pellet was resuspended in nuclear extraction buffer, vortexed, and centrifuged, and the supernatant (nuclear extract) was prepared. For plasma membrane isolation, cells were collected and resuspended in 0.2 mM EDTA in 1 mM $NaHCO_3$ in an approximate ratio of 1 ml/10^8 cells and incubated on ice for 30 min to swell the cells. Cells were homogenized using a Dounce homogenizer. The homogenates were centrifuged for 10 min at 175 × *g* at 4 °C to remove unbroken cells and nuclei, and the supernatant was centrifuged at 25,000 × *g* for 30 min at 4 °C to prepare a plasma membrane–enriched microsome fraction. The supernatant was discarded, and the pellets were resuspended in 0.2 M potassium phosphate buffer, pH 7.2. The resuspended membranes then were loaded onto the two-phase system with a polymer mixture containing 6.6% Dextran T500 (GE Healthcare), 6.6% (w/w) poly(ethylene glycol) 3350 (Fisher Scientific), and 0.2 M potassium phosphate, pH 7.2. The phases were separated by centrifugation at 1150 × *g* for 5 min at 4 °C. The upper phase containing primarily plasma membranes was collected.

Gene transfer

For ORP4L knockdown, high-titer lentivirus carrying shRNA (TCAGAGTCAAGCTCAGGTGTA) prepared by Shanghai GenePharma (Shanghai, China) was used. 1 × 10^6 cells were resuspended in 100 μl of medium with lentivirus (multiplicity of infection, 100) and 5 μg ml^{-1} Polybrene in a 24-well culture plate. Infections were carried out for 6 h at 37 °C in 5% CO_2. At the end of infection, 400 μl of medium was added. Efficacy of knockdown of ORP4L was verified by Western blotting after 3-day infection. A 4D-Nucleofector™ System (Lonza, Basel, Switzerland) was used for transient transfection of ORP4L, ORP4L ΔFFAT, and ORP4L ΔFFAT&ORD constructs and VAPA siRNA (catalogue number sc-61768, Santa Cruz Biotechnology) in Jurkat T-cells.

Coimmunoprecipitation and GST pulldown assay

For the coimmunoprecipitation assay, 1 × 10^7 Jurkat T-cells were washed twice with ice-cold PBS and incubated on ice for 30 min with 1 ml of lysis buffer (50 mM Tris-Cl, 150 mM NaCl, 0.5 mM $MgCl_2$, 10% glycerol, and 0.5% Triton X-100, pH 8.0) supplemented with protease inhibitor mixture (Roche Applied Science). Cell lysates were centrifuged for 15 min at 15,000 × *g*. The supernatant was preabsorbed with 50 μl of Protein G–agarose (Invitrogen) for 1 h at 4 °C. The recovered supernatant was incubated overnight with VAPA or control antibody at 4 °C. 50 μl of Protein G–agarose was added to the lysate-antibody mixture and incubated for 2 h at 4 °C on a roller. The beads were washed four times with lysis buffer and boiled in SDS-PAGE loading buffer. Samples were resolved on 10% SDS-polyacrylamide gels and subjected to Western blot analysis with antibodies.

For GST pulldown assay, pGEX-4T-1 (Addgene, Cambridge, MA), full-length ORP4L constructs (pGEX-4T-1-ORP4L), or the truncated ORP4L constructs lacking the FFAT motif (pGEX-4T-1-ORP4L ΔFFAT) were transformed into *E. coli* Rosetta™ (DE3) (Novagen) and cultured at 37 °C to A_{600} 0.5–1.0 followed by induction with 0.1 mM isopropyl 1-thio-β-D-galactopyranoside for 16–18 h at 18 °C. The cells were collected, and crude bacterial lysates were prepared by sonication in lysis buffer 1 (50 mM Tris-Cl, 150 mM NaCl, 1% Triton X-100, and 1 mM phenylmethylsulfonyl fluoride, pH 8.0) in the presence of the protease inhibitor mixture (Roche Applied Science). Bacterial lysates were centrifuged for 20 min at 12,000 × *g*, and the supernatants were used for fusion protein purification with GST-Bind beads (Novagen) according to the manufacturer's protocol. Jurkat T-cells were washed twice with cold PBS, lysed in lysis buffer, and shaken for 30 min on ice, and the lysate was cleared by a 10-min centrifugation at 12,000 rpm in a microcentrifuge. For pulldown, 10 μg of GST/GST-ORP4L/GST-ORP4L ΔFFAT and 30 μl of GST-Bind beads were incubated for 30 min on ice followed by washing three times with PBS. Jurkat T-cells lysates were then added and incubated at 4 °C overnight. Then the beads were washed three times with lysis buffer, resuspended into 2× SDS-PAGE loading buffer at 98 °C for 5 min, and resolved on 10% SDS-polyacrylamide gels for Western blotting.

Measurement of RAN activity

RAN activity was measured using a RAN activation assay kit according to the manufacturer's instructions (NewEast Biosciences). Briefly, anti-active RAN mouse mAb was incubated with cell lysates containing RAN-GTP. The bound active RAN was pulled down by Protein A/G–agarose, eluted, and detected by immunoblot analysis using polyclonal rabbit anti-Ran antibody.

Determination of phospholipase C activity

Phospholipase C activity was analyzed using the EnzChek® Direct Phospholipase C Assay kit (Molecular Probes) according to the manufacturer's instructions.

Measurement of IP_3 production

IP_3 was measured using an ELISA kit for IP_3 (CEC037Ge, Cloud-Clone Corp.) according to the manufacturer's instructions. Briefly, 0.5 × 10^6 Jurkat T-cells transfected with the indicated construct were lysed with lysis buffer and incubated with Detection Reagent A for 1 h at 37 °C. After aspirating and washing three times, Detection Reagent B was added, incubated for 30 min at 37 °C, then aspirated, and washed five times. Substrate Solution was added and incubated for 7 min at 37 °C. Finally, the reactions were blocked with Stop Solution and read at 450 nm immediately.

Ca^{2+} imaging

Cells (0.5 × 10^6 cells ml^{-1}) transfected with the indicated construct were plated onto glass-bottomed dishes and incubated with 1 μM Fluo-4-AM for 30 min at 37 °C in ECB buffer (130 mM NaCl, 5 mM KCl, 1.5 mM $CaCl_2$, 1 mM $MgCl_2$, 25 mM Hepes, pH 7.5, 1 mg ml^{-1} BSA, and 5 mM glucose). The buffer was replaced, and incubation continued for 20 min at 37 °C to permit dye de-esterification. Culture dishes were mounted on the stage of an inverted confocal microscope (Olympus FV3000 laser-scanning confocal microscope system) equipped with a 40× objective. Calcium measurements were performed in fresh ECB buffer at 37 °C with 5% CO_2. The Ca^{2+} images of

cells excited with low-intensity 488-nm laser excitation were acquired at 2-s intervals alternately under time-lapse mode. Image data were subsequently analyzed using ImageJ (National Institutes of Health) and are presented as a ratio of F/F_0 in the final results where F_0 represents baseline fluorescence intensity in each cell.

Immunofluorescence microscopy

Cells were seeded onto coverslips, stimulated with anti-CD3 for the indicated times, and then fixed with 4% paraformaldehyde for 30 min at room temperature followed by permeabilization with 0.1% Triton X-100 for 5 min and blocking with 10% FBS for 30 min at room temperature. Cells were then incubated with primary antibodies in 5% FBS at 4 °C overnight. After washing three times (10 min each) with PBS, cells were incubated with fluorescent secondary antibody conjugates at 37 °C for 30 min followed by staining with Hoechst 33342 at room temperature for 10 min. Finally, the specimens were analyzed using a Zeiss LSM 510 Meta laser-scanning confocal microscope system or Olympus FV3000 laser-scanning confocal microscope system.

Western blot analysis

Cellular total protein samples were mixed with loading sample buffer, boiled for 10 min, and subjected to SDS-PAGE followed by transfer onto polyvinylidene difluoride membranes (Millipore, Life Science). After blocking and incubations of the membranes with primary antibodies and HRP–secondary antibody conjugates (Bio-Rad), the blots were developed by enhanced chemiluminescence (Millipore, Life Science). Proteins were quantified by densitometry using ImageJ (National Institutes of Health), and the data were normalized using the β-actin signal.

Statistical analyses

All data are expressed as mean ± S.D. of at least three independent experiments. Differences between groups were analyzed by unpaired two-tailed Student's t test. p values of <0.05 were considered statistically significant.

Author contributions—G. P., X. C., C. Lai, and W. Z. data curation; G. P. software; G. P. validation; G. P., B. L., C. Li, and J. Z. visualization; G. P. and W. Z. methodology; X. C., C. Li, and D. L. investigation; V. M. O. and W. Z. conceptualization; V. M. O., W. Z., and D. Y. writing-original draft; W. Z. supervision; W. Z. and D. Y. project administration; D. Y. funding acquisition.

References

1. Cocco, L., Martelli, A. M., Gilmour, R. S., Rhee, S. G., and Manzoli, F. A. (2001) Nuclear phospholipase C and signaling. *Biochim. Biophys. Acta* **1530,** 1–14 CrossRef Medline
2. Thomas, G. M., Cunningham, E., Fensome, A., Ball, A., Totty, N. F., Truong, O., Hsuan, J. J., and Cockcroft, S. (1993) An essential role for phosphatidylinositol transfer protein in phospholipase C-mediated inositol lipid signaling. *Cell* **74,** 919–928 CrossRef Medline
3. Putney, J. W., and Bird, G. S. (2008) Cytoplasmic calcium oscillations and store-operated calcium influx. *J. Physiol.* **586,** 3055–3059 CrossRef Medline
4. Ramazzotti, G., Faenza, I., Gaboardi, G. C., Piazzi, M., Bavelloni, A., Fiume, R., Manzoli, L., Martelli, A. M., and Cocco, L. (2008) Catalytic activity of nuclear PLC-β_1 is required for its signalling function during C2C12 differentiation. *Cell. Signal.* **20,** 2013–2021 CrossRef Medline
5. Divecha, N., and Irvine, R. F. (1995) Phospholipid signaling. *Cell* **80,** 269–278 CrossRef Medline
6. Faenza, I., Bavelloni, A., Fiume, R., Santi, P., Martelli, A. M., Maria Billi, A., Lo Vasco, V. R., Manzoli, L., and Cocco, L. (2004) Expression of phospholipase Cβ family isoenzymes in C2C12 myoblasts during terminal differentiation. *J. Cell. Physiol.* **200,** 291–296 CrossRef Medline
7. Taylor, F. R., Saucier, S. E., Shown, E. P., Parish, E. J., and Kandutsch, A. A. (1984) Correlation between oxysterol binding to a cytosolic binding protein and potency in the repression of hydroxymethylglutaryl coenzyme A reductase. *J. Biol. Chem.* **259,** 12382–12387 Medline
8. Lehto, M., Laitinen, S., Chinetti, G., Johansson, M., Ehnholm, C., Staels, B., Ikonen, E., and Olkkonen, V. M. (2001) The OSBP-related protein family in humans. *J. Lipid Res.* **42,** 1203–1213 Medline
9. Im, Y. J., Raychaudhuri, S., Prinz, W. A., and Hurley, J. H. (2005) Structural mechanism for sterol sensing and transport by OSBP-related proteins. *Nature* **437,** 154–158 CrossRef Medline
10. Suchanek, M., Hynynen, R., Wohlfahrt, G., Lehto, M., Johansson, M., Saarinen, H., Radzikowska, A., Thiele, C., and Olkkonen, V. M. (2007) The mammalian oxysterol-binding protein-related proteins (ORPs) bind 25-hydroxycholesterol in an evolutionarily conserved pocket. *Biochem. J.* **405,** 473–480 CrossRef Medline
11. Tong, J., Yang, H., Yang, H., Eom, S. H., and Im, Y. J. (2013) Structure of Osh3 reveals a conserved mode of phosphoinositide binding in oxysterol-binding proteins. *Structure* **21,** 1203–1213 CrossRef Medline
12. Levine, T. P., and Menon, A. K. (2013) A protein pair with PIPs inside. *Structure* **21,** 1070–1071 CrossRef Medline
13. Mesmin, B., Bigay, J., Moser von Filseck, J., Lacas-Gervais, S., Drin, G., and Antonny, B. (2013) A four-step cycle driven by PI(4)P hydrolysis directs sterol/PI(4)P exchange by the ER-Golgi tether OSBP. *Cell* **155,** 830–843 CrossRef Medline
14. Kentala, H., Pfisterer, S. G., Olkkonen, V. M., and Weber-Boyvat, M. (2015) Sterol liganding of OSBP-related proteins (ORPs) regulates the subcellular distribution of ORP-VAPA complexes and their impacts on organelle structure. *Steroids* **99,** 248–258 CrossRef Medline
15. Kaiser, S. E., Brickner, J. H., Reilein, A. R., Fenn, T. D., Walter, P., and Brunger, A. T. (2005) Structural basis of FFAT motif-mediated ER targeting. *Structure* **13,** 1035–1045 CrossRef Medline
16. Loewen, C. J., Roy, A., and Levine, T. P. (2003) A conserved ER targeting motif in three families of lipid binding proteins and in Opi1p binds VAP. *EMBO J.* **22,** 2025–2035 CrossRef Medline
17. Wang, P. Y., Weng, J., and Anderson, R. G. (2005) OSBP is a cholesterol-regulated scaffolding protein in control of ERK 1/2 activation. *Science* **307,** 1472–1476 CrossRef Medline
18. Yan, D., and Olkkonen, V. M. (2008) Characteristics of oxysterol binding proteins. *Int. Rev. Cytol.* **265,** 253–285 CrossRef Medline
19. Lev, S., Ben Halevy, D., Peretti, D., and Dahan, N. (2008) The VAP protein family: from cellular functions to motor neuron disease. *Trends Cell Biol.* **18,** 282–290 CrossRef Medline
20. Wyles, J. P., and Ridgway, N. D. (2004) VAMP-associated protein-A regulates partitioning of oxysterol-binding protein-related protein-9 between the endoplasmic reticulum and Golgi apparatus. *Exp. Cell Res.* **297,** 533–547 CrossRef Medline
21. Fournier, M. V., Guimarães da Costa, F., Paschoal, M. E., Ronco, L. V., Carvalho, M. G., and Pardee, A. B. (1999) Identification of a gene encoding a human oxysterol-binding protein-homologue: a potential general molecular marker for blood dissemination of solid tumors. *Cancer Res.* **59,** 3748–3753 Medline
22. Henriques Silva, N., Vasconcellos Fournier, M., Pimenta, G., Pulcheri, W. A., Spector, N., and da Costa Carvalho Mda, G. (2003) HLM/OSBP2 is expressed in chronic myeloid leukemia. *Int. J. Mol. Med.* **12,** 663–666 Medline
23. Burgett, A. W., Poulsen, T. B., Wangkanont, K., Anderson, D. R., Kikuchi, C., Shimada, K., Okubo, S., Fortner, K. C., Mimaki, Y., Kuroda, M., Murphy, J. P., Schwalb, D. J., Petrella, E. C., Cornella-Taracido, I., Schirle, M.,

et al. (2011) Natural products reveal cancer cell dependence on oxysterol-binding proteins. *Nat. Chem. Biol.* **7,** 639–647 CrossRef Medline
24. Zhong, W., Yi, Q., Xu, B., Li, S., Wang, T., Liu, F., Zhu, B., Hoffmann, P. R., Ji, G., Lei, P., Li, G., Li, J., Li, J., Olkkonen, V. M., and Yan, D. (2016) ORP4L is essential for T-cell acute lymphoblastic leukemia cell survival. *Nat. Commun.* **7,** 12702 CrossRef Medline
25. Moore, M. S., and Blobel, G. (1994) A G protein involved in nucleocytoplasmic transport: the role of Ran. *Trends Biochem. Sci.* **19,** 211–216 CrossRef Medline
26. Avis, J. M., and Clarke, P. R. (1996) Ran, a GTPase involved in nuclear processes: its regulators and effectors. *J. Cell Sci.* **109,** 2423–2427 Medline
27. Kalderon, D., Roberts, B. L., Richardson, W. D., and Smith, A. E. (1984) A short amino acid sequence able to specify nuclear location. *Cell* **39,** 499–509 CrossRef Medline
28. Di Ventura, B., and Kuhlman, B. (2016) Go in! Go out! Inducible control of nuclear localization. *Curr. Opin. Chem. Biol.* **34,** 62–71 CrossRef Medline
29. Nguyen Ba, A. N., Pogoutse, A., Provart, N., and Moses, A. M. (2009) NLStradamus: a simple hidden Markov model for nuclear localization signal prediction. *BMC Bioinformatics* **10,** 202 CrossRef Medline
30. la Cour, T., Kiemer, L., Mølgaard, A., Gupta, R., Skriver, K., and Brunak, S. (2004) Analysis and prediction of leucine-rich nuclear export signals. *Protein Eng. Des. Sel.* **17,** 527–536 CrossRef Medline
31. Zhong, W., Pan, G., Wang, L., Li, S., Ou, J., Xu, M., Li, J., Zhu, B., Cao, X., Ma, H., Li, C., Xu, J., Olkkonen, V. M., Staels, B., and Yan, D. (2016) ORP4L facilitates macrophage survival via G-protein-coupled signaling: ORP4L−/− mice display a reduction of atherosclerosis. *Circ. Res.* **119,** 1296–1312 CrossRef Medline
32. Yue, C., and Sanborn, B. M. (2001) KN-93 inhibition of G protein signaling is independent of the ability of Ca^{2+}/calmodulin-dependent protein kinase II to phosphorylate phospholipase Cβ3 on 537-Ser. *Mol. Cell. Endocrinol.* **175,** 149–156 CrossRef Medline
33. Moore, M. S. (1998) Ran and nuclear transport. *J. Biol. Chem.* **273,** 22857–22860 CrossRef Medline
34. Fornerod, M., Ohno, M., Yoshida, M., and Mattaj, I. W. (1997) CRM1 is an export receptor for leucine-rich nuclear export signals. *Cell* **90,** 1051–1060 CrossRef Medline
35. Fukuda, M., Asano, S., Nakamura, T., Adachi, M., Yoshida, M., Yanagida, M., and Nishida, E. (1997) CRM1 is responsible for intracellular transport mediated by the nuclear export signal. *Nature* **390,** 308–311 CrossRef Medline
36. Stefan, C. J., Manford, A. G., Baird, D., Yamada-Hanff, J., Mao, Y., and Emr, S. D. (2011) Osh proteins regulate phosphoinositide metabolism at ER-plasma membrane contact sites. *Cell* **144,** 389–401 CrossRef Medline
37. Toulmay, A., and Prinz, W. A. (2011) Lipid transfer and signaling at organelle contact sites: the tip of the iceberg. *Curr. Opin. Cell Biol.* **23,** 458–463 CrossRef Medline
38. Rhee, S. G., Suh, P. G., Ryu, S. H., and Lee, S. Y. (1989) Studies of inositol phospholipid-specific phospholipase C. *Science* **244,** 546–550 CrossRef Medline
39. Ghai, R., Du, X., Wang, H., Dong, J., Ferguson, C., Brown, A. J., Parton, R. G., Wu, J. W., and Yang, H. (2017) ORP5 and ORP8 bind phosphatidylinositol-4,5-biphosphate (PtdIns(4,5)P_2) and regulate its level at the plasma membrane. *Nat. Commun.* **8,** 757 CrossRef Medline
40. Martelli, A. M., Billi, A. M., Gilmour, R. S., Neri, L. M., Manzoli, L., Ognibene, A., and Cocco, L. (1994) Phosphoinositide signaling in nuclei of Friend cells: phospholipase Cβ down-regulation is related to cell differentiation. *Cancer Res.* **54,** 2536–2540 Medline
41. Manzoli, L., Billi, A. M., Gilmour, R. S., Martelli, A. M., Matteucci, A., Rubbini, S., Weber, G., and Cocco, L. (1995) Phosphoinositide signaling in nuclei of Friend cells: tiazofurin down-regulates phospholipase Cβ1. *Cancer Res.* **55,** 2978–2980 Medline
42. Zini, N., Martelli, A. M., Cocco, L., Manzoli, F. A., and Maraldi, N. M. (1993) Phosphoinositidase C isoforms are specifically localized in the nuclear matrix and cytoskeleton of Swiss 3T3 cells. *Exp. Cell Res.* **208,** 257–269 CrossRef Medline
43. Wang, S., Lukinius, A., Zhou, Y., Stålberg, P., Gobl, A., Oberg, K., and Skogseid, B. (2000) Subcellular distribution of phospholipase C isoforms in rodent pancreas and gastric mucosa. *Endocrinology* **141,** 2589–2593 CrossRef Medline
44. Golub, T., and Caroni, P. (2005) PI(4,5)P_2-dependent microdomain assemblies capture microtubules to promote and control leading edge motility. *J. Cell Biol.* **169,** 151–165 CrossRef Medline
45. Berberián, G., Forcato, D., and Beaugé, L. (2009) Key role of a PtdIns-4,5P2 micro domain in ionic regulation of the mammalian heart Na^+/Ca^{2+} exchanger. *Cell Calcium* **45,** 546–553 CrossRef Medline
46. Gamper, N., and Shapiro, M. S. (2007) Target-specific PIP_2 signalling: how might it work? *J. Physiol.* **582,** 967–975 CrossRef Medline
47. Levine, T., and Loewen, C. (2006) Inter-organelle membrane contact sites: through a glass, darkly. *Curr. Opin. Cell Biol.* **18,** 371–378 CrossRef Medline
48. Wu, M. M., Buchanan, J., Luik, R. M., and Lewis, R. S. (2006) Ca^{2+} store depletion causes STIM1 to accumulate in ER regions closely associated with the plasma membrane. *J. Cell Biol.* **174,** 803–813 CrossRef Medline
49. Luik, R. M., Wu, M. M., Buchanan, J., and Lewis, R. S. (2006) The elementary unit of store-operated Ca^{2+} entry: local activation of CRAC channels by STIM1 at ER-plasma membrane junctions. *J. Cell Biol.* **174,** 815–825 CrossRef Medline